Breakdown of effective-medium theory in dielectric composites containing epsilon-near-zero constituents

Ran Mei,[1,3] Jin Qin,[2] Dongyang Yan,[1,3] Yun Lai,[2,*] and Jie Luo[1,3,†]

[1]*Institute of Theoretical and Applied Physics, School of Physical Science and Technology, Soochow University, Suzhou 215006, China*

[2]*National Laboratory of Solid State Microstructures, School of Physics, and Collaborative Innovation Center of Advanced Microstructures, Nanjing University, Nanjing 210093, China*

[3]*Provincial Key Lab of Thin Films, Soochow University, Suzhou 215006, China*

(Received 5 August 2023; accepted 12 December 2023; published 2 January 2024)

Dielectric composites are believed to tightly obey the effective-medium theory (EMT) when their dimensions are much smaller compared to the wavelength inside them. It is naturally expected that when the refractive indices of a part of the constituent materials approach zero, the validity of the EMT is further strengthened. Here, we demonstrate that the EMT breaks down in deep-subwavelength dielectric composites containing homogeneous epsilon-near-zero (ENZ) constituents, which is contrary to the above intuitive picture, as validated by both the Bloch-wave analysis and numerical simulations. This breakdown of EMT originates in the presence of strong evanescent waves emerging on the interfaces between the constituent materials, which stem from the extreme mismatch of energy-flux distributions between them. The energy flux within such composites is highly nonuniform: significantly enhanced in the ENZ constituents and largely depressed in other normal constituents. When such composites are illuminated by planar waves with uniform energy-flux distributions, evanescent waves for redistributing flux into the ENZ constituents are generated on the internal interfaces of the composites, and lead to properties beyond the prediction of traditional EMT. Our work unveils the mechanism of EMT breakdown in dielectric composites with constituents of near-zero permittivity.

DOI: 10.1103/PhysRevB.109.045104

I. INTRODUCTION

Intermixing two or more homogeneous constituents to form composite materials is a fundamental approach for constructing advanced electromagnetic/optical materials, including metamaterials [1,2], which enable unprecedented control of electromagnetic waves and light. When the dimensions of the constituents are much smaller than the wavelength, i.e., at the deep-subwavelength scale, the composite can usually be homogenized as an effective medium with uniform properties, which is described by effective-medium theories (EMTs) [3–5]. Generally, local EMTs are sufficient for accurately describing the macroscopic electromagnetic/optical responses. They predict the macroscopic effective permittivity/permeability of the composite in terms of the permittivities/permeabilities and filling fractions of the individual constituents, disregarding their actual dimensions and spatial arrangement [3–5]. This homogenization process greatly simplifies the modeling, characterization, and phenomenological understanding of the composite material.

Dielectric composite materials with deeply subwavelength constituents, which cannot support extremely large wave vectors or surface-wave resonances, are generally believed to obey the local EMT [3–5]. Interestingly, exceptional cases where the local EMT fundamentally breaks down were discovered recently. Sheinfux *et al.* [6] demonstrated that the transmission through a one-dimensional (1D) dielectric multilayer depends strongly on nanoscale variations at the vicinity of the effective medium's critical angle for total internal reflection, revealing the breakdown of EMT [7–15]. The EMT fails in this scenario because it cannot account for the influence of microscopic evanescent waves in low-index dielectric layers [6,7]. Dong *et al.* [16] further revealed the breakdown of EMT in two- and three-dimensional (2D and 3D) systems. In contrast to the 1D systems, the breakdown of EMT is caused by the occurrence of dramatically varying evanescent fields at the deep-subwavelength scale, which however are ignored or averaged out in the effective-medium description.

Typically, reducing the refractive index of a part of the constituents to nearly zero can increase the effective wavelength in the composite; therefore, it is generally expected that this would alleviate the breakdown of EMT and strengthen the validity of EMT. However, in this work, we report a contrasting finding: the breakdown of EMT in deeply subwavelength dielectric composites containing homogeneous constituents with permittivity approaching zero, i.e., epsilon-near-zero (ENZ) media. Such homogeneous ENZ media can be realized using conductive materials at plasma frequency [17–22] and waveguide metamaterials at cutoff frequency [23–28]. Due to their unique electromagnetic properties, such as infinitely long wavelength, zero phase advancement, and extreme impedance, a plethora of novel phenomena has been discovered, including tunneling effect [23], electromagnetic flux control [27,29], photonic doping and antidoping

*laiyun@nju.edu.cn
†luojie@suda.edu.cn

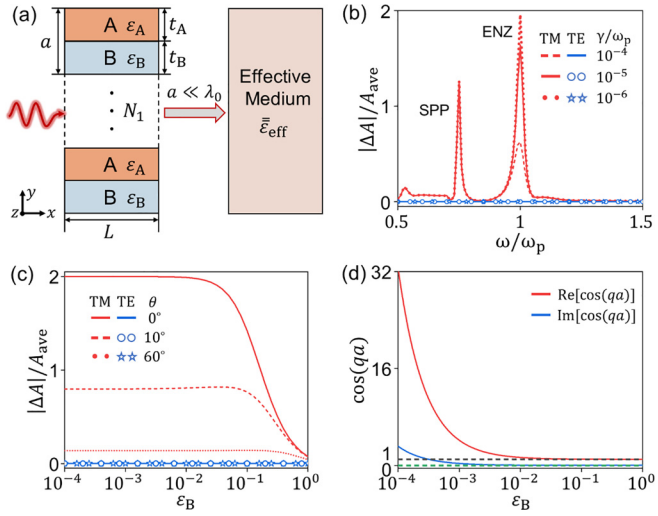

FIG. 1. (a) Schematic graph of a deep-subwavelength 1D multilayer consisting of alternating layers of nonmagnetic materials A and B, which can be homogenized as a uniform medium characterized by an effective relative permittivity tensor $\bar{\bar{\varepsilon}}_{\text{eff}}$. (b), (c) Relative difference of absorptance $|\Delta A|/A_{\text{ave}}$ between the actual multilayer and its effective medium for TM (red) and TE (blue) waves. In (b), the incident angle θ is fixed at 0°, while the angular frequency ω and the damping frequency γ are changed. The relevant parameters are $\varepsilon_A = 2 + 0.2i$, $\varepsilon_B = 1-\omega_p^2/(\omega^2 + i\omega\gamma)$, $t_A = t_B = \lambda_0/100$, and $L = \lambda_0$. In (c), we set $\gamma = 0$, and change the ε_B and θ. (d) The real and imaginary parts of $\cos(qa)$ as the function of ε_B for propagation of $k_{\parallel} = k_0$ based on the dispersion relation in Eq. (1).

[24–26,30], nonlinearity enhancement and quenching effect [20–22,31], unusual waveguiding effect [28], etc.

Here, we find that when a dielectric composite contains homogeneous ENZ constituents at the deep-subwavelength scale, its macroscopic properties could deviate from the prediction of local EMT, as validated by both the Bloch-wave analysis and numerical simulations. We demonstrate that the EMT breakdown is attributed to the occurrence of strong evanescent waves at the interface between the constituents. The continuity of the electric displacement and magnetic field across the interfaces between ENZ and other constituents can result in significantly enhanced energy flux in the ENZ constituents and suppressed energy flux in other normal constituents. Consequently, a highly nonuniform energy-flux distribution within the composite is formed. To match with the uniform energy-flux distribution of incident waves, strong evanescent waves that can transversely transfer flux from the normal constituents to the ENZ constituents are generated. Such evanescent waves are beyond the description of the traditional EMT. Our work enriches the understanding of EMT in describing composites containing ENZ constituents.

II. BREAKDOWN OF EMT IN MULTILAYERS CONTAINING ENZ CONSTITUENTS

We begin with a 1D multilayer comprising alternating layers of nonmagnetic materials A (relative permittivity ε_A, thickness t_A) and B (relative permittivity ε_B, thickness t_B), as illustrated in Fig. 1(a). According to the EMT, when the multilayer operates at the deep-subwavelength scale, meaning that the lattice constant a $(= t_A + t_B)$ is much smaller than the incident wavelength λ_0 in free space, it can be homogenized as a uniform medium characterized by an effective relative permittivity tensor $\bar{\bar{\varepsilon}}_{\text{eff}} = \begin{pmatrix} \varepsilon_{x,\text{eff}} & & \\ & \varepsilon_{y,\text{eff}} & \\ & & \varepsilon_{z,\text{eff}} \end{pmatrix}$, where $\varepsilon_{x,\text{eff}} = \varepsilon_{z,\text{eff}} = (\varepsilon_A t_A + \varepsilon_B t_B)/a$ and $\varepsilon_{y,\text{eff}} = \varepsilon_A \varepsilon_B a/(\varepsilon_A t_B + \varepsilon_B t_A)$ [5].

To numerically examine the validity of the effective-medium approximation, we set $t_A = t_B = a/2 = \lambda_0/100$, ensuring that the condition $a \ll \lambda_0$ is satified. Here, we assume that the material A is dissipative characterized by a complex relative permittivity of $\varepsilon_A = 2 + 0.2i$, and then compare the absorptance of the actual multilayer A^{ML} and its effective medium A^{EMT} using finite-element software COMSOL MULTIPHYSICS. The relative permittivity of material B is characterized by the Drude model as $\varepsilon_B = 1-\omega_p^2/(\omega^2 + i\omega\gamma)$, where ω_p and γ are the plasma frequency and damping frequency, respectively. Figure 1(b) presents the relative difference of absorptance $|\Delta A|/A_{\text{ave}}$ as the function of normalized angular frequency ω/ω_p for transverse-electric (TE, electric field along the z direction) and transverse-magnetic (TM, magnetic field along the z direction) polarized waves under normal incidence (i.e., the incident angle $\theta = 0°$) for different γ. Here, $\Delta A = A^{\text{ML}} - A^{\text{EMT}}$ and $A_{\text{ave}} = (A^{\text{ML}} + A^{\text{EMT}})/2$. The length of the multilayer is $L = \lambda_0$ along the x direction. From Fig. 1(b), it is observed that the absorptance difference is negligibly small for TE waves. This indicates the validity of the EMT in accurately describing the multilayer structure. Since the TE waves only interact with the effective-permittivity component $\varepsilon_{z,\text{eff}}$, these results confirm the accuracy of the effective-permittivity components parallel to the A-B interface (i.e., $\varepsilon_{x,\text{eff}}$ and $\varepsilon_{z,\text{eff}}$).

Nevertheless, notable differences in absorption are observed for TM waves at $\omega = 0.71\omega_p$ and $\omega = \omega_p$, which correspond to $\varepsilon_B \sim -1$ and $\varepsilon_B \sim 0$, respectively. It is known that the discrepancy at $\omega = 0.71\omega_p$ is caused by the excitation of surface plasmon polariton (SPP) resonances at the A-B interfaces [32–34]. At the SPP frequency, the EMT generally breaks down and fails to accurately describe the multilayer structure [32–34]. Interestingly, a greater discrepancy occurs at $\omega = \omega_p$, i.e., the ENZ frequency. We see that the $|\Delta A|/A_{\text{ave}}$ increases as the damping loss decreases, and reaches a maximal value of 2 when $\gamma \leqslant 10^{-6}\omega_p$. A value of $|\Delta A|/A_{\text{ave}} = 2$ means that either $A^{\text{ML}} \gg A^{\text{EMT}}$ or $A^{\text{EMT}} \gg A^{\text{ML}}$, indicating the breakdown of the EMT. Through numerical calculations, we find that $A^{\text{ML}} \gg A^{\text{EMT}}$ at the ENZ frequency.

To investigate the physical mechanism underlying the breakdown of EMT at the ENZ frequency, we consider ideal cases by setting $\gamma = 0$ in the following, and explore the effects of the value of ε_B on the $|\Delta A|/A_{\text{ave}}$. Figure 1(c) shows the calculated $|\Delta A|/A_{\text{ave}}$ as the function of ε_B for TE and TM waves under different incident angles. Still, the EMT is accurate for TE waves, while it breaks down for TM waves. It is seen that the $|\Delta A|/A_{\text{ave}}$ for TM waves increases rapidly as ε_B approaches zero, and reaches a maximal value of 2 when $\varepsilon_B < 10^{-2}$. Considering that the normally incident TM waves only interact with $\varepsilon_{y,\text{eff}}$, the discrepancy between the actual structure and its effective medium indicates the inaccuracy

of $\varepsilon_{y,\text{eff}}$ and the breakdown of EMT in the presence of ENZ constituents. We note that the breakdown of EMT is mitigated when the incident angle increases. It is expected because with a larger incident angle, a greater portion of electric field is polarized along the x direction, for which the formula of the effective permittivity component (i.e., $\varepsilon_{x,\text{eff}}$) is accurate.

The breakdown of EMT at the ENZ frequency is predictable based on the analysis of Bloch waves. By utilizing the transfer matrix method and the Bloch theorem, the dispersion relation of the multilayer structure for TM waves is expressed as [6,33]

$$\cos(qa) = \cos(q_A t_A)\cos(q_B t_B) - \frac{1}{2}\left(\frac{\varepsilon_A q_B}{\varepsilon_B q_A} + \frac{\varepsilon_B q_A}{\varepsilon_A q_B}\right)\sin(q_A t_A)\sin(q_B t_B), \quad (1)$$

where $q_{A,B} = \sqrt{\varepsilon_{A,B}k_0^2 - k_\parallel^2}$, and q is the Bloch wave number. k_0 is the wave number in free space, and $k_\parallel$ is the parallel component of wave vector at the A-B interfaces. The applicability of the EMT requires that the wavelength of the Bloch wave is much larger than the lattice constant; in other words, $qa \ll 1$. This criterion leads to

$$\cos(qa) \sim 1. \quad (2)$$

Generally, for deeply subwavelength multilayer structures that do not support extremely large wave vectors or surface-wave resonances, the condition of Eq. (2) can be well satisfied, and the EMT can be safely applied in the homogenization of the multilayers. However, the dispersion relation that determines $\cos(qa)$ contains not only phase shifts across the layers, but also the impedance ratios of the two adjacent layers. When the constituent B is made of ENZ materials (i.e., $\varepsilon_B \sim 0$), Eq. (1) simplifies to

$$\cos(qa) \sim 1 + \frac{1}{2}\frac{\varepsilon_A}{\varepsilon_B}k_\parallel^2 t_A t_B, \quad (3)$$

for the case of $k_\parallel \neq 0$. Equation (3) indicates that the EMT would fail to accurately describe the multilayers containing ENZ constituents.

For numerical investigation, in Fig. 1(d) we plot the real and imaginary parts of $\cos(qa)$ as the function of ε_B for propagation of $k_\parallel = k_0$ according to the dispersion relation in Eq. (1). It is seen that the value of $\cos(qa)$ gradually deviates from unity as the ε_B approaches zero. Specifically, the deviation becomes significant when $\varepsilon_B < 10^{-2}$. This indicates that the EMT breaks down when $\varepsilon_B < 10^{-2}$, consistent with the results in Fig. 1(c). These results clearly manifest the breakdown of EMT in the presence of ENZ constituents, and highlight the critical role of impedance ratios of the two adjacent layers.

III. THE UNDERLYING PHYSICS OF EMT BREAKDOWN

To further explore the physical mechanism responsible for the breakdown of EMT, we compare the field distributions within the actual multilayer and its effective medium. We first consider the case of normally incident TE waves, as depicted in Fig. 2(a). For the multilayer at the deep-subwavelength scale, the fields can be considered uniform within each constituent [4,5]. By applying the continuity boundary conditions

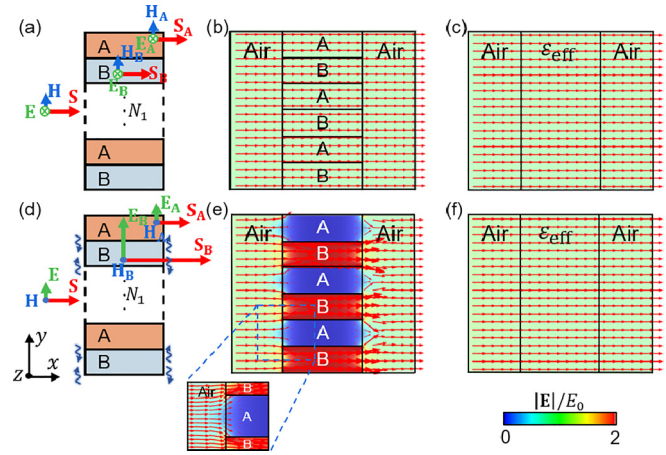

FIG. 2. (a), (d) Illustration of electric field $\mathbf{E}$, magnetic field $\mathbf{H}$, and Poynting vector $\mathbf{S}$ inside the deep-subwavelength multilayer under the illumination of normally incident (a) TE and (d) TM waves. The blue wavy arrows in (d) denote the evanescent waves. (b), (c), (e), and (f) Distributions of normalized electric field $|\mathbf{E}|/E_0$ and time-averaged energy flux $\bar{\mathbf{S}}$ (arrows) in the models of (b), (e) actual multilayer; (c), (f) effective medium for normally incident (b),(c) TE and (e), (f) TM waves. The inset of (e) shows the enlarged view of field distributions at the air-multilayer interface. The relevant parameters are $\varepsilon_A = 2 + 0.2i$, $\varepsilon_B = 10^{-4}$, and $t_A = t_B = \lambda_0/100$.

for the tangential electric field and normal component of magnetic induction at the A-B interfaces, we find that the electric field $\mathbf{E}_A$ and magnetic field $\mathbf{H}_A$ in the A layers are equal to the electric field $\mathbf{E}_B$ and magnetic field $\mathbf{H}_B$ in the B layers, respectively. Hence, we have $\mathbf{E}_A = \mathbf{E}_B$ and $\mathbf{H}_A = \mathbf{H}_B$, indicating that the energy flux, denoted as $\mathbf{S} = \mathbf{E} \times \mathbf{H}$, is uniformly distributed throughout the multilayer, i.e., $\mathbf{S}_A = \mathbf{S}_B$. For numerical verification, Fig. 2(b) displays the distributions of normalized electric field $|\mathbf{E}|/E_0$ (color) and time-averaged energy flux $\bar{\mathbf{S}}$ ($= \frac{1}{2}\text{Re}(\mathbf{E} \times \mathbf{H}^*)$, depicted as arrows, within a multilayer slab with $L = 0.03\lambda_0$ when it is illuminated by normally incident TE waves from air. Here, E_0 is the electric field maginitude of incidence, and the relavant parameters are set as $\varepsilon_A = 2 + 0.2i$, $\varepsilon_B = 10^{-4}$, and $t_A = t_B = \lambda_0/100$. Uniform electric field and energy flux are clearly observed inside the multilayer, exhibiting good agreement with the field distributions in its effective medium characterized by $\varepsilon_{z,\text{eff}} = 1.000\,05 + 0.1i$ [Fig. 2(c)]. This further corroborates the validity of the effective-medium approximation for TE waves.

Interestingly, the behavior of TM waves is markedly different. By considering the continuity conditions for the normal component of electric displacement field and magnetic field at the A-B interfaces, we find that $\mathbf{E}_A = (\varepsilon_B/\varepsilon_A)\mathbf{E}_B$ and $\mathbf{H}_A = \mathbf{H}_B$. In the case where the B layers are made of ENZ media with $\varepsilon_B \to 0$, we have $\mathbf{E}_B \gg \mathbf{E}_A \to 0$ and $\mathbf{S}_B \gg \mathbf{S}_A \to 0$ [Fig. 2(d)]. This indicates extremely nonuniform distributions of electric fields and energy flux within the multilayer. Specifically, the electric fields and energy flux are substantially large in the A layers, while they approach zero in the B layers, as confirmed by the simulation results in Fig. 2(e). These highly nonuniform field distributions completely contradict the uniform field distribu-

tions predicted by the effective-medium model with $\varepsilon_{y,\text{eff}} = 0.0002 + 9.9 \times 10^{-10} i$ [Fig. 2(f)]. Consequently, the EMT fails to accurately characterize the multilayer structure for TM waves.

We note that the energy flux of the incident planar waves in free space is uniformly distributed on the yz plane. When these waves impinge upon the yz surface of the multilayer structure, a significant discrepancy arises in the energy-flux distributions at the air-multilayer interface. This contradiction would give rise to strong evanescent waves that decay in the forward and backward directions (i.e., $\pm x$ direction), but are capable of transferring flux from the normal (or ENZ) constituents to the ENZ (or normal) constituents along the perpendicular direction (i.e., $\pm y$ direction) at the left (or right) air-multilayer interface, as schematically shown by the blue wavy arrows in Fig. 2(d). These evanescent waves produce rapidly varying evanescent fields at the air-multilayer interfaces, and enhance the electric fields in the A layers where the material loss exists. In contrast, in the effective-medium scenario, the electric field and energy flux should be totally concentrated in the ENZ layers (i.e., the B layers). Consequently, wave absorption in the actual multilayer is significantly greater than that in its effective medium counterpart, as observed in Fig. 1(b). These findings clearly demonstrate that the breakdown of EMT is attributed to the presence of evanescent waves at the air-multilayer interfaces, which are induced by the extreme mismatch of energy-flux distributions.

To provide further evidence on the role that evanescent waves play in the EMT breakdown, we compare the wave absorption of two models, denoted as models I and II, as schematically shown in Fig. 3(a). Model I consists of a continuous multilayer slab (N_1 number of AB units in the y direction, and length L in the x direction) placed in air (upper-panel graph). Subsequently, we divide the multilayer slab equally into N_2 thin multilayer slabs, each having a length of $l = L/N_2$ along the x direction (lower-panel graph). Two adjacent thin multilayer slabs are separated by an air slab with a separation distance of g.

Figure 3(b) presents the absorptance of the two models and their corresponding effective-medium models (where all multilayer slabs are replaced by the effective medium) as the function of L/λ_0 while keeping λ_0 fixed under the illumination of normally incident TM waves. In model II, the length of each thin multilayer slab is fixed at $l = \lambda_0/100$. The parameters are $\varepsilon_A = 2 + 0.2i$, $\varepsilon_B = 10^{-4}$, $t_A = t_B = \lambda_0/100$, and $g = l$. From Fig. 3(b), we see that the two effective-medium models exhibit nearly the same absorptance, which however is several orders of magnitude lower than that of their actual multilayer models. This apparent contradiction highlights the breakdown of EMT. Furthermore, it is notable that the absorptance of model I remains almost unchanged as the length L. This is due to the fact that the number of air-multilayer interfaces, where the absorption occurs, does not increase proportionally. Interestingly, by dividing the continuous multilayer slab into multiple thin slabs in model II, a significant increase in absorptance is achieved since a large number of air-multilayer interfaces are created. As expected, the absorptance in model II is two orders of magnitude higher than that in model I, and it further increases with increasing the length L, as shown in Fig. 3(b).

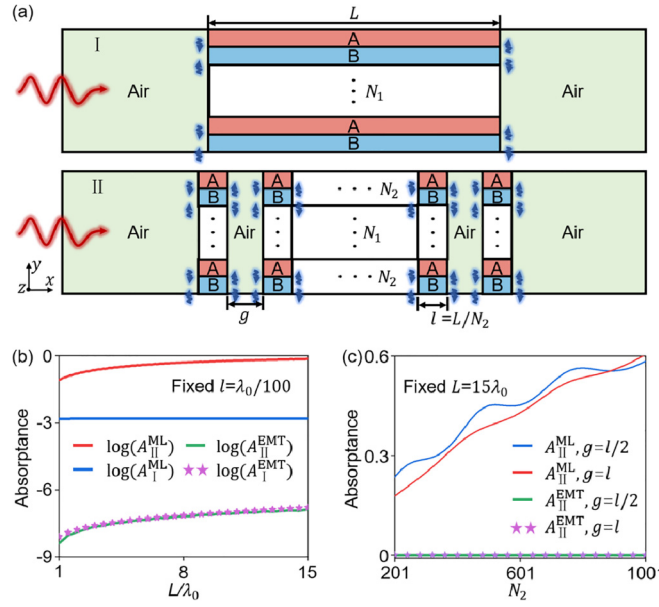

FIG. 3. (a) Upper: schematic graph of wave propagation through model I consisting of a continuous multilayer slab (N_1 number of AB units in the y direction, length L in the x direction) in air background under normally incident TM illumination. Lower: in model II the multilayer slab is equally divided into N_2 thin multilayer slabs, each having a length of $l = L/N_2$ along the x direction. Two adjacent thin slabs are separated by an air slab with a separation distance of g. The blue wavy arrows denote the evanescent waves. (b) Absorptance on a log scale for the model I (A_{I}^{ML}) and model II ($A_{\text{II}}^{\text{ML}}$), as well as their corresponding effective-medium models ($A_{\text{I}}^{\text{EMT}}$ and $A_{\text{II}}^{\text{EMT}}$) as the function of L/λ_0 with fixed λ_0. In model II, each thin multilayer slab has a fixed length of $l = \lambda_0/100$. (c) Absorptance of the model II and its corresponding effective model as the function of N_2 for different separation distances: $g = l$ and $g = l/2$. The total length of all thin multilayer slabs is fixed at $L = N_2 l = 15\lambda_0$. In (b) and (c), the relevant parameters are $\varepsilon_A = 2 + 0.2i$, $\varepsilon_B = 10^{-4}$, and $t_A = t_B = \lambda_0/100$.

Additionally, we keep the total length of all thin multilayer slabs in model II fixed at $L = 15\lambda_0$, and vary the number N_2. Figure 3(c) presents the absorptance of the actual multilayer and its effective-medium model for two different separation distances: $g = l$ and $g = l/2$. It is seen that the absorption of the effective-medium model is negligibly small and shows little dependence on the separation distance. In contrast, the absorption of the actual multilayer is significantly higher. We note that the separation distance affects the absorption because the evanescent waves at adjacent interfaces could couple with each other if the air gap were sufficiently small. Although the absorptance varies for different separation distances, we observe the same increasing trend with N_2, as the number of air-multilayer interfaces increases. These results provide further evidence that the evanescent waves at the air-multilayer interfaces are responsible for the breakdown of EMT.

IV. THREE-DIMENSIONAL COMPOSITES CONTAINING ENZ CONSTITUENTS

The breakdown of EMT occurs due to the generation of strong evanescent waves by the ENZ constituents in

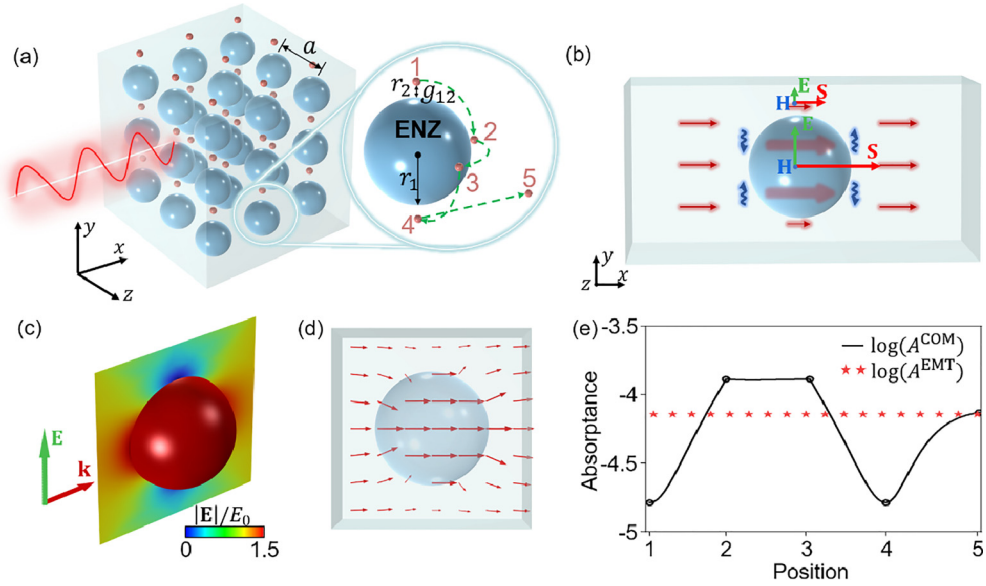

FIG. 4. (a) Schematic graph of a 3D deep-subwavelength composite consisting of a cubic lattice of a large ENZ spherical particle and a small lossy dielectric spherical particle in air background. The green dashed curve denotes the trajectory of the small particle moving around the ENZ particle. Positions 1 and 4 are close to the poles, positions 2 and 3 are on the equatorial plane, and position 5 is far from the ENZ particle. (b) Illustration of electric field **E**, magnetic field **H**, and Poynting vector **S** inside the composite. The blue wavy arrows denote the evanescent waves. (c), (d) Distributions of (c) normalized electric field amplitude $|\mathbf{E}|/E_0$ on the xy plane and the ENZ particle's surface, and (d) time-averaged energy flux $\bar{\mathbf{S}}$ in one unit cell in the absence of the small particle. (e) Absorptance of the actual composite slab consisting of 100 units along the x direction A^{COM} (black lines) and its effective medium A^{EMT} (red stars) as the function of the position of the small particle along the trajectory in (a).

composites at the deep-subwavelength scale. This physical mechanism underlying the EMT breakdown is not limited to 1D multilayer systems but can also be observed in 2D and 3D composites. In the following, we will show the evanescent-wave-induced breakdown of EMT in a 3D composite containing the ENZ constituents.

Figure 4(a) illustrates the schematic graph of the 3D composite, which consists of a cubic lattice (lattice constant $a = \lambda_0/100$) of a large ENZ spherical particle (radius $r_1 = 0.3a$, relative permittivity $\varepsilon_1 = 10^{-3}$) and a small lossy dielectric spherical particle (radius $r_2 = 0.03a$, relative permittivity $\varepsilon_2 = 2 + 0.2i$) embedded in an air background. The edge-to-edge distance between the two particles is g_{12}. The position of the small particle is adjustable and can be moved along the trajectory $1 \to 2 \to 3 \to 4 \to 5$ [green dashed curves in Fig. 4(a)]. Since the composite operates at the deep-subwavelength scale, it can be homogenized as a uniform effective medium. The effective relative permittivity $\varepsilon_{\mathrm{eff}}$ can be obtained through solving the equation $\frac{\varepsilon_{\mathrm{eff}}-1}{\varepsilon_{\mathrm{eff}}+2} = \frac{4\pi}{3a^3}\left(r_1^3\frac{\varepsilon_1-1}{\varepsilon_1+2} + r_2^3\frac{\varepsilon_2-1}{\varepsilon_2+2}\right)$ [5].

Here, we consider planar waves with electric fields polarized along the y direction, which are normally incident onto the yz surface of the composite. According to the continuity condition for electric displacement field at the poles of the ENZ particle, the electric field inside the ENZ particle is significantly larger than that in the surrounding air, as depicted in Fig. 4(b) and confirmed by the simulation results in Fig. 4(c). Consequently, the energy flux inside the ENZ particle is much greater than that in the nearby air region close to the poles of the ENZ particle, as evidenced by the simulated time-averaged energy-flux distributions in Fig. 4(d). This leads to the formation of a nonuniform energy-flux distribution in the vicinity of the ENZ particle. When planar waves are incident onto the composite, evanescent waves capable of transversely transferring flux from the nearby air region (or ENZ particle) to the ENZ particle (or nearby air region) on the left (or right) side will be generated. These evanescent waves give rise to rapidly varying evanescent fields in the vicinity of the ENZ particle. Specifically, the electric field on the ENZ sphere's surface on the air side can be derived as $E_{\mathrm{air}} = \frac{3}{2}E_0\cos\theta$ based on the Mie scattering theory or the electrostatic theory [31]. Here, θ is the polar angle (the angle measured from the x axis). This implies that the electric field is enhanced (i.e., $E_{\mathrm{air}} = \frac{3}{2}E_0$) on the equator (i.e., $\theta = 0$), while is zero (i.e., $E_{\mathrm{air}} = 0$) at the poles (i.e., $\theta = \pi/2$). Under this circumstance, the nearby small lossy particle would experience dramatically different local fields at different positions, leading to position-dependent absorption.

To demonstrate this phenomenon, Fig. 4(e) shows the absorptance of the actual composite slab (black lines), consisting of 100 units along the x direction, when the small particle is successively moved from position 1 to position 5 along the trajectory illustrated in Fig. 4(a). Along the trajectory $1 \to 4$, the edge-to-edge distance g_{12} is kept unchanged at $0.03a$, while at position 5, the edge-to-edge distance g_{12} is $0.44a$. From Fig. 4(e), apparent position-dependent absorption is observed in the actual composite, which however, is absent in the effective medium model (red stars). This disparity indicates the breakdown of EMT. The EMT breaks down in this scenario because it fails to capture the intricate details of the evanescent fields at the deep-subwavelength scale, thereby resulting in an

inaccurate description of the 3D composites containing ENZ constituents.

V. DISCUSSION AND CONCLUSION

It was discovered that evanescent waves occurring in composites could disrupt the validity of EMT in accurately describing their macroscopic electromagnetic/optical responses even when they are at the deep-subwavelength scale [6–15,32–34]. Strong evanescent waves are generally expected to occur in metal-dielectric composites due to the excitation of surface plasmon polaritons [32–34], and in all-dielectric multilayer structures at the vicinity of the effective medium's critical angle for total internal reflection [6–15]. Interestingly, our work demonstrates the occurrence of dramatic evanescent waves in dielectric composites containing ENZ constituents under normal incidence, thus unveiling a mechanism of EMT breakdown.

From the perspective of Bloch waves, the breakdown of EMT can also be attributed to the extreme impedance ratios of the two adjacent layers. For normal dielectric materials, such extreme impedance ratios are generally unattainable, as unnaturally high permittivity of materials is required. Simultaneously, the introduction of such high-permittivity materials could break the deep-subwavelength condition. Interestingly, our work demonstrates a feasible route towards deeply subwavelength multilayers with extreme impedance contrast between adjacent layers, i.e., by utilizing ENZ materials. Since the proposed multilayers are SPP-free and do not support any surface-wave resonance, the inapplicability of EMT is generally unexpected.

Finally, it is noteworthy that our findings apply to homogeneous ENZ media. This is because the evanescent waves that lead to the breakdown of EMT occur at the deep-subwavelength scale, where composite ENZ materials [35–38] generally fail to exhibit their effective ENZ responses due to complicated microstructures. Actually, the influences of the microstructures on the formation of evanescent waves and the applicability of EMT to the composites containing composite ENZ constituents are still unclear, and worthy of further exploration.

In summary, we have demonstrated the breakdown of EMT in composites containing homogeneous ENZ constituents, even at the deep-subwavelength scale. This breakdown is attributed to the presence of strong evanescent waves at the interfaces between the constituents. These evanescent waves emerge due to the significant mismatch of energy-flux distributions. Our findings challenge the conventional understanding that the validity of EMT is enhanced when the effective wavelength becomes longer, thus providing a deeper comprehension for wave behaviors at the deep-subwavelength scale.

Data underlying the results presented in this paper are not publicly available at this time but may be obtained from the authors upon reasonable request.

ACKNOWLEDGMENTS

This work was supported by National Natural Science Foundation of China (Grants No. 12374293, No. 12174188, and No. 11974176), National Key R&D Program of China (Grants No. 2022YFA1404303 and No. 2020YFA0211300), Natural Science Foundation of Jiangsu Province (Grant No. BK20221354), and Undergraduate Training Program for Innovation and Entrepreneurship, Soochow University.

The authors declare no conflicts of interest.

[1] D. R. Smith, J. B. Pendry, and M. C. Wiltshire, Metamaterials and negative refractive index, Science **305**, 788 (2004).

[2] T. J. Cui, D. R. Smith, and R. Liu, *Metamaterials: Theory, Design, and Applications* (Springer, New York, 2010).

[3] J. C. Maxwell Garnett, Colours in metal glasses and in metallic films, Philos. Trans. R. Soc. A **203**, 385 (1904).

[4] K. Dolgaleva and R. W. Boyd, Local-field effects in nanostructured photonic materials, Adv. Opt. Photonics **4**, 1 (2012).

[5] V. A. Markel, Introduction to the Maxwell Garnett approximation: Tutorial, J. Opt. Soc. Am. A **33**, 1244 (2016).

[6] H. Herzig Sheinfux, I. Kaminer, Y. Plotnik, G. Bartal, and M. Segev, Subwavelength multilayer dielectrics: Ultrasensitive transmission and breakdown of effective-medium theory, Phys. Rev. Lett. **113**, 243901 (2014).

[7] S. V. Zhukovsky, A. Andryieuski, O. Takayama, E. Shkondin, R. Malureanu, F. Jensen, and A. V. Lavrinenko, Experimental demonstration of effective medium approximation breakdown in deeply subwavelength all-dielectric multilayers, Phys. Rev. Lett. **115**, 177402 (2015).

[8] H. Herzig Sheinfux, I. Kaminer, A. Z. Genack, and M. Segev, Interplay between evanescence and disorder in deep subwavelength photonic structures, Nat. Commun. **7**, 12927 (2016).

[9] V. Popov, A. V. Lavrinenko, and A. Novitsky, Operator approach to effective medium theory to overcome a breakdown of Maxwell Garnett approximation, Phys. Rev. B **94**, 085428 (2016).

[10] X. Lei, L. Mao, Y. Lu, and P. Wang, Revisiting the effective medium approximation in all-dielectric subwavelength multilayers: Breakdown and rebuilding, Phys. Rev. B **96**, 035439 (2017).

[11] H. H. Sheinfux, Y. Lumer, G. Ankonina, A. Z. Genack, G. Bartal, and M. Segev, Observation of Anderson localization in disordered nanophotonic structures, Science **356**, 953 (2017).

[12] A. Maurel and J. Marigo, Sensitivity of a dielectric layered structure on a scale below the periodicity: A fully local homogenized model, Phys. Rev. B **98**, 024306 (2018).

[13] M. Coppolaro, G. Castaldi, and V. Galdi, Effects of deterministic disorder at deeply subwavelength scales in multilayered dielectric metamaterials, Opt. Express **28**, 10199 (2020).

[14] M. A. Gorlach and M. Lapine, Boundary conditions for the effective-medium description of subwavelength multilayered structures, Phys. Rev. B **101**, 075127 (2020).

[15] M. Coppolaro, G. Castaldi, and V. Galdi, Anomalous light transport induced by deeply subwavelength quasiperiodicity

in multilayered dielectric metamaterials, Phys. Rev. B **102**, 075107 (2020).

[16] T. Dong, J. Luo, H. Chu, X. Xiong, R. Peng, M. Wang, and Y. Lai, Breakdown of Maxwell Garnett theory due to evanescent fields at deep-subwavelength scale, Photonics Res. **9**, 848 (2021).

[17] D. C. Adams, S. Inampudi, T. Ribaudo, D. Slocum, S. Vangala, N. A. Kuhta, W. D. Goodhue, V. A. Podolskiy, and D. Wasserman, Funneling light through a subwavelength aperture with epsilon-near-zero materials, Phys. Rev. Lett. **107**, 133901 (2011).

[18] S. Vassant, A. Archambault, F. Marquier, F. Pardo, U. Gennser, A. Cavanna, J. L. Pelouard, and J. J. Greffet, Epsilon-near-zero mode for active optoelectronic devices, Phys. Rev. Lett. **109**, 237401 (2012).

[19] J. Kim, A. Dutta, G. V. Naik, A. J. Giles, F. J. Bezares, C. T. Ellis, J. G. Tischler, A. M. Mahmoud, H. Caglayan, and O. J. Glembocki, Role of epsilon-near-zero substrates in the optical response of plasmonic antennas, Optica **3**, 339 (2016).

[20] M. Z. Alam, I. De Leon, and R. W. Boyd, Large optical nonlinearity of indium tin oxide in its epsilon-near-zero region, Science **352**, 795 (2016).

[21] Y. Yang, J. Lu, A. Manjavacas, T. S. Luk, H. Liu, K. Kelley, J. Maria, E. L. Runnerstrom, M. B. Sinclair, S. Ghimire, and I. Brener, High-harmonic generation from an epsilon-near-zero material, Nat. Phys. **15**, 1022 (2019).

[22] W. Jia, M. Liu, Y. Lu, X. Feng, Q. Wang, X. Zhang, Y. Ni, F. Hu, M. Gong, X. Xu, Y. Huang, W. Zhang, Y. Yang, and J. Han, Broadband terahertz wave generation from an epsilon-near-zero material, Light: Sci. Appl. **10**, 11 (2021).

[23] B. Edwards, A. Alù, M. Young, M. Silveirinha, and N. Engheta, Experimental verification of epsilon-near-zero metamaterial coupling and energy squeezing using a microwave waveguide, Phys. Rev. Lett. **100**, 033903 (2008).

[24] I. Liberal, A. M. Mahmoud, Y. Li, B. Edwards, and N. Engheta, Photonic doping of epsilon-near-zero media, Science **355**, 1058 (2017).

[25] M. Coppolaro, M. Moccia, G. Castaldi, N. Engheta, and V. Galdi, Non-Hermitian doping of epsilon-near-zero media, Proc. Natl. Acad. Sci. USA **117**, 13921 (2020).

[26] Z. Zhou, H. Li, W. Sun, Y. He, I. Liberal, N. Engheta, Z. Feng, and Y. Li, Dispersion coding of ENZ media via multiple photonic dopants, Light: Sci. Appl. **11**, 207 (2022).

[27] W. Ji, J. Luo, and Y. Lai, Extremely anisotropic epsilon-near-zero media in waveguide metamaterials, Opt. Express **27**, 19463 (2019).

[28] W. Ji, J. Luo, H. Chu, X. Zhou, X. Meng, R. Peng, M. Wang, and Y. Lai, Crosstalk prohibition at the deep-subwavelength scale by epsilon-near-zero claddings, Nanophotonics **12**, 2007 (2023).

[29] J. Luo, W. Lu, Z. Hang, H. Chen, B. Hou, Y. Lai, and C. T. Chan, Arbitrary control of electromagnetic flux in inhomogeneous anisotropic media with near-zero index, Phys. Rev. Lett. **112**, 073903 (2014).

[30] J. Luo, J. Li, and Y. Lai, Electromagnetic impurity-immunity induced by parity-time symmetry, Phys. Rev. X **8**, 031035 (2018).

[31] C. Wang, R. Shi, L. Gao, A. S. Shalin, and J. Luo, Quenching of second-harmonic generation by epsilon-near-zero media, Photonics Res. **11**, 1437 (2023).

[32] A. V. Chebykin, A. A. Orlov, A. V. Vozianova, S. I. Maslovski, Y. S. Kivshar, and P. A. Belov, Nonlocal effective medium model for multilayered metal-dielectric metamaterials, Phys. Rev. B **84**, 115438 (2011).

[33] J. Luo, H. Chen, B. Hou, P. Xu, and Y. Lai, Nonlocality-induced negative refraction and subwavelength imaging by parabolic dispersions in metal-dielectric multilayered structures with effective zero permittivity, Plasmonics **8**, 1095 (2013).

[34] R. Pollard, A. Murphy, W. Hendren, P. Evans, R. Atkinson, G. Wurtz, A. Zayats, and V. Podolskiy, Optical nonlocalities and additional waves in epsilon-near-zero metamaterials, Phys. Rev. Lett. **102**, 127405 (2009).

[35] R. Liu, Q. Cheng, T. Hand, J. Mock, T. Cui, S. Cummer, and D. Smith, Experimental demonstration of electromagnetic tunneling through an epsilon-near-zero metamaterial at microwave frequencies, Phys. Rev. Lett. **100**, 023903 (2008).

[36] R. Maas, J. Parsons, N. Engheta, and A. Polman, Experimental realization of an epsilon-near-zero metamaterial at visible wavelengths, Nat. Photonics **7**, 907 (2013).

[37] X. Huang, Y. Lai, Z. H. Hang, H. Zheng, and C. T. Chan, Dirac cones induced by accidental degeneracy in photonic crystals and zero-refractive-index materials, Nat. Mater. **10**, 582 (2011).

[38] D. Yan, R. Mei, M. Li, Z. Ma, Z. H. Hang, and J. Luo, Controlling coherent perfect absorption via long-range connectivity of defects in three-dimensional zero-index media, Nanophotonics **12**, 4195 (2023).